AGU100 ADVANCING EARTH AND SPACE SCIENCE

Water Resources Research

RESEARCH ARTICLE
10.1029/2018WR023383

Key Points:
- We present full solution to stochastic water hammer equations
- It provides significant computational gain over Monte Carlo
- It is suitable for Bayesian data assimilation for leak detection

Correspondence to:
D. M. Tartakovsky,
tartakovsky@stanford.edu

Citation:
Alawadhi, A., Boso, F., & Tartakovsky, D. M. (2018). Method of distributions for water hammer equations with uncertain parameters. *Water Resources Research*, *54*, 9398–9411. https://doi.org/10.1029/2018WR023383

Received 25 MAY 2018
Accepted 30 SEP 2018
Accepted article online 11 OCT 2018
Published online 26 NOV 2018

Method of Distributions for Water Hammer Equations With Uncertain Parameters

Abdulrahman Alawadhi[1], Francesca Boso[2], and Daniel M. Tartakovsky[2]

[1]Department of Mechanical and Aerospace Engineering, University of California, San Diego, La Jolla, CA, USA, [2]Department of Energy Resources Engineering, Stanford University, Stanford, CA, USA

Abstract Water hammer equations (WHE) are routinely used to interpret leak detection tests in pipe networks. Assimilation of pressure data into model predictions is typically done within the probabilistic framework, which treats uncertain model parameters (e.g., initial and boundary conditions, location, and intensity of a leak) as random variables so that solutions of the WHE are given in terms of probability density functions (PDFs) of fluid pressure and velocity. These are usually estimated with computationally expensive Monte Carlo simulations. We use the method of distributions to derive a deterministic equation for the (joint) PDFs of the pressure and flow rate governed by the WHE. This PDF equation employs a closure approximation that ensures the self-consistency in terms of the mean and variance of the state variables. Our numerical experiments demonstrate the agreement between solutions of the PDF equation and Monte Carlo simulations, and the computational efficiency of the former relative to the latter.

1. Introduction

Pipe networks are the main way for transporting fluids (e.g., water and hydrocarbons) from a reservoir to their final destination. However, as pipes age, they become prone to leakage due to corrosion. This raises environmental concerns and impacts public health when contaminants enter a compromised water distribution system or hydrocarbons spill into the ambient environment. Leaks also lead to economical losses due to wasted resources and repair costs. The World Bank estimates the global "nonrevenue" water, due to real and apparent losses and unbilled authorized consumption, to be worth $14.7 billion per year (Thornton et al., 2008); real water losses in distribution and transmission systems operated by water utilities are between 20% and 50% (Brothers, 2001). Localization and quantification of such losses are critical for monitoring the reliability of pipe networks and planning repairs.

Since leakage affects pressure and flow rate in a pipe, comparison between measurements of these quantities in a compromised pipe with their counterparts in the intact pipe could, in principle, be used to identify the location and intensity of a leak. However, each pipe in a network rarely contains more than one pressure gauge, so that pressure values at any location along a pipe (with and without a leak) must be inferred from an appropriate model. Practical and financial constraints on the number and positioning of measurement devices within a pipe network often result in the data being collected only upstream of a maneuver valve. Even if pressure measurements were available along the length of a pipe, the leak localization from steady-state pressure measurements would not be accurate. Consequently, transient test-based techniques were developed, mostly for single pipes (transmission mains) but also for laboratory pipe systems used to mimic distribution networks (Meniconi et al., 2015).

A popular leak-detection test involves an abrupt valve closure; it creates a contact-discontinuity wave moving upstream of the valve, which conveys information about fluid pressure and velocity to a sensor. This hydraulic regime is described by the cross-sectionally averaged Navier-Stokes equations, which are called the *water hammer equations* or WHE (Chaudhry, 2013; Wylie et al., 1993). This experimental setup for leak detection and its interpretations with the WHE are reviewed in considerable detail by Colombo et al. (2009). (An alternative strategy, in which pressure waves along the pipes are generated by means of water injection (Brunone et al., 2008; Taghvaei et al., 2010), is not considered in this study.) Relevant techniques for identification of a leak's location and intensity can be subdivided into forward methods (Brunone & Ferrante, 2001; Wang et al., 2002) and inverse methods in the time (Massari et al., 2013; Vítkovskỳ et al., 2007) and frequency (Covas et al., 2005; Mpesha et al., 2001) domains. In the first class of the inverse methods, several pressure transducers installed in

the pipe system provide measurements that are used to calibrate possibly very complex models of pressure and flow throughout the distribution system. In the second class, time or frequency pressure signals measured at a single location are analyzed as the system responds to a perturbation by comparing these readings to the no-leak conditions.

Predictability of WHE-based models and their use in conjunction with data are undermined by both uncertainty in the model parameters and measurement errors. Within the probabilistic framework both uncertain parameters and noisy data are treated as random quantities, and probabilistic model predictions are reported in terms of probability density functions (PDFs) of pressure and velocity or, more often, their ensemble means and (co)variances. These PDFs provide a complete probabilistic description of fluid flow in a pipe, including assessment of probabilities of rate events, and serve to quantify predictive uncertainty of WHE-based models. Probabilistic solutions of the WHE are also needed for identification of leaks and blockages in pipes by means of stochastic successive linear estimator (Massari et al., 2014) or data assimilation techniques based on Kalman filter (Ye & Fenner, 2010).

Probabilistic solutions of the WHE can be obtained with Monte Carlo simulations (MCS Duan, 2015; Zhang et al., 2011). This method is robust and easy to implement but suffers from slow convergence and correspondingly high computational cost. If input parameters have large correlation lengths, polynomial chaos expansions (Sattar & El-Beltagy, 2016) are often, but not always (Barajas-Solano & Tartakovsky, 2016), more efficient than MCS. The first-order perturbation analysis (e.g., Neuman et al., 1996) provides yet another alternative to MCS, which is appropriate for small variances of the input parameters and yields the means and variances of system states; it has been used in the WHE context by Massari et al. (2013, 2014). Our goal is to derive and solve deterministic equations for the (joint) PDFs of pressure head and flow velocity governed by the stochastic WHE, while avoiding linearization of the latter and accounting for shocks.

The stochastic WHE are formulated in section 2; they describe spatiotemporal evolution of cross-sectionally averaged fluid pressure head, $h(x,t)$, and velocity, $u(x,t)$, in a pipe following an abrupt closure of a valve. In section 3, we derive a deterministic equation for the joint PDF of these two state variables, f_{hu}, which provides a full probabilistic description of the system's behavior at any point x along the pipe at any time t. In section 4, we report a series of numerical experiments that demonstrate the accuracy and computational efficiency of this PDF equation by comparing its solution with the corresponding PDF estimated with MCS. Major conclusions drawn from this study are summarized in section 5.

2. Problem Formulation

We consider a pipe of length L and diameter D that is equipped with a pressure sensor at $x = x^\star$ and a shut-off valve at the outlet $x = L$ (Figure 1); it forms a part of a distribution network. Steady-state fluid flow in the pipe is pressure driven, with the inlet pressure head H_{in} exceeding the outlet pressure head H_{out} ($H_{\text{in}} > H_{\text{out}}$). A water hammer test is often conducted in an attempt to identify the location ($x = x_{\text{leak}}$) and intensity (Q_{leak}) of a leak. The leak intensity is defined as $Q_{\text{leak}}(h) = C_{\text{leak}} A_{\text{leak}} \sqrt{2gh} = \gamma_{\text{leak}} \sqrt{h}$, where C_{leak} and A_{leak} are the coefficient and area of discharge, respectively, and $\gamma_{\text{leak}} = C_{\text{leak}} A_{\text{leak}} \sqrt{2g}$. The test consists of an instantaneous, at time $t = 0$, shutoff of the flow at the outlet, $u(x = L, t > 0) = 0$, and observing the pressure transients at the sensor.

Cross-sectionally averaged pressure head, $h(x,t)$, and velocity, $u(x,t)$, of the resulting turbulent flow in the pipe ($0 < x < L$) are governed by the (hyperbolic partial differential) WHE (Chaudhry, 2013; Wylie et al., 1993),

$$\frac{\partial h}{\partial t} + \frac{a^2}{g}\frac{\partial u}{\partial x} = Q_{\text{leak}}\delta(x - x_{\text{leak}}) \tag{1a}$$

$$\frac{\partial u}{\partial t} + g\frac{\partial h}{\partial x} = k|u|u, \qquad k = -\frac{f}{2D} \tag{1b}$$

where a is the wave speed, g is the gravitational acceleration, and f is Darcy-Weisbach friction factor. These equations describe the dynamics of contact discontinuities moving back and forth between the inlet and outlet (Figure 1). The simplified model (1) relies on a quasi steady-state approximation of the wall shear stress (equating it to the squared local velocity), but the methodology presented below can also handle unsteady friction formulations.

These equations are subject to boundary conditions

$$h(x = 0, t) = H_{\text{in}} \qquad \text{and} \qquad u(x = L, t) = 0. \tag{2a}$$

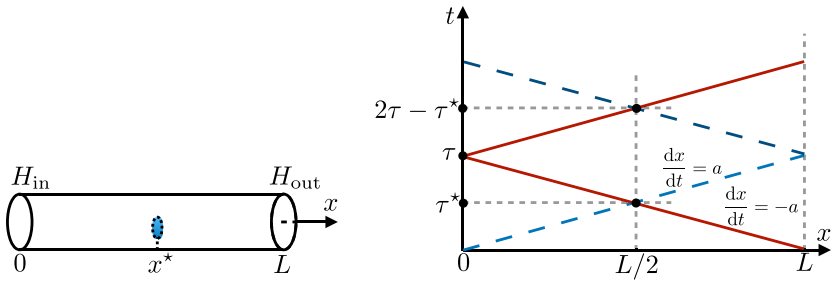

Figure 1. (left) A pipe of length L equipped with a pressure sensor and a valve located at $x = x^\star$ and $x = L$, respectively. At steady state, that is, with the open valve, flow is driven by the difference in hydraulic heads at the inlet, H_{in}, and the outlet, H_{out}. (right) The contact discontinuities (waves), induced by the instantaneous (at time $t = 0$) closure of the valve, propagate with wave speed a along two families of characteristics defined by $\mathrm{d}x/\mathrm{d}t = a$ and $\mathrm{d}x/\mathrm{d}t = -a$. The first contact discontinuity, traveling backward from the shut valve, reaches the sensor's location $x^\star = L/2$ at time $\tau^\star = L/(2a)$, and the pipe's inlet ($x = 0$) at time $\tau = L/a$. At that time, it turns into the second contact discontinuity that travels forward, reaching the sensor's location at time $2\tau - \tau^\star$.

The initial conditions for both u and h correspond to the steady-state condition of the system. It has a spatially uniform velocity u_0 and a spatially varying pressure head h_0, which is related to u_0 by the steady state WHE,

$$h_0(x; u_0) = \frac{k}{g}|u_0|u_0 x + H_{\text{in}}. \tag{2b}$$

The initial value u_0 is uncertain and treated as a random variable with prescribed PDF $f_{u_0}(U_0)$; the latter quantifies, for example, the probability of u_0 not exceeding any given value U_0.

Consequently, predictions of $u(x, t)$ and $h(x, t)$ based on (1)–(2) are uncertain as well; their probabilistic description at a space-time point (x, t) is given by the joint PDF $f_{uh}(U, H; x, t)$. It can be used to compute, for example, the probability of both flow velocity u exceeding a certain value U and pressure head h exceeding a certain value H. Estimating $f_{uh}(U, H; x, t)$ with MCS is computationally expensive, and often prohibitively so, if one has to reassemble an exhaustive set of MC runs for each potential leak location x_{leak}.

3. PDF Solutions to WHEs

The main result of this study is the derivation in Appendix A of a deterministic equation for the PDF $f_{uh}(U, H; x, t)$,

$$\frac{\partial f_{uh}}{\partial t} + \tilde{\nabla} \cdot (\mathbf{V} f_{uh}) = 0, \tag{3a}$$

where $\tilde{\nabla} = (\partial/\partial H, \partial/\partial U)^\top$ is the del operator in the phase space (H, U) of f_{uh}, and $\mathbf{V} = (V_H, V_U)^\top$ is the phase-space velocity with components

$$V_H = -\frac{a^2}{g}\frac{\partial \bar{u}}{\partial x} + Q_{\text{leak}}(H)\delta(x - x_{\text{leak}}) + \alpha_1(H - \bar{h}), \qquad V_U = -g\frac{\partial \bar{h}}{\partial x} + \alpha_2(U - \bar{u}) + k|U|U. \tag{3b}$$

Here $\bar{u}(x, t)$ and $\bar{h}(x, t)$ are the ensemble means (averages) of random $u(x, t)$ and $h(x, t)$, respectively; $\sigma_u^2(x, t)$ and $\sigma_h^2(x, t)$ are their respective variances; and the coefficients α_1 and α_2 are given by (Appendix A)

$$\alpha_1 = -\frac{\gamma_{\text{leak}}\delta\left(x - x_{\text{leak}}\right)}{2\sqrt{\bar{h}}} + \frac{1}{2}\frac{\partial \ln \sigma_h^2}{\partial t} \qquad \text{and} \qquad \alpha_2 = -2k|\bar{u}| + \frac{1}{2}\frac{\partial \ln \sigma_u^2}{\partial t}. \tag{3c}$$

As demonstrated below, these statistics are computed with MCS at the fraction of the computational cost required to generate an MC sample sufficient for accurate estimation of the full PDF.

Probabilistic predictions of the pressure head $h(x, t)$ and flow velocity $u(x, t)$ separately are encapsulated in the marginal PDFs $f_u(U; x, t)$ and $f_h(H; x, t)$. These are defined from the joint PDF f_{uh} as $f_u(U; x, t) = \int f_{uh}\mathrm{d}H$ and $f_h(H; x, t) = \int f_{uh}\mathrm{d}U$. They satisfy the PDF equations

$$\frac{\partial f_h}{\partial t} + \frac{\partial V_H f_h}{\partial H} = 0 \tag{4}$$

and

$$\frac{\partial f_u}{\partial t} + \frac{\partial V_U f_u}{\partial U} = 0, \tag{5}$$

which are derived by integrating (3) over U and H, respectively.

Joint/marginal PDF equations (3)–(5) are subject to initial and boundary conditions that reflect the information about the initial and boundary conditions of the physical system. Specifically, the initial condition for (3) is given in terms of the joint PDF of the initial states u_0 and h_0, $f_{u_0h_0}(U,H;x)$. Given f_{u_0}, the marginal PDF of u_0, the latter is expressed in terms of the conditional PDF $f_{h_0|u_0}$ as $f_{u_0h_0} = f_{h_0|u_0}f_{u_0}$. Since (2) provides a deterministic relation between u_0 and h_0, knowledge of the former completely determines the latter, that is, $f_{h_0|u_0} = \delta(H - h_0)$.

Since PDF equations (3)–(5) do not contain spatial derivatives, the space coordinate x acts as a parameter. Consequently, one can obtain the PDFs of u and h only at points where they are needed for data assimilation, for example, where the pressure sensors are deployed.

4. Simulation Results

In the simulations reported below, we consider fluid flow in a pipe of length $L = 3{,}000$ m and diameter $D = 0.5$ m, and with the Darcy-Weisbach friction factor $f = 0.03$. An instantaneous closure of the valve at the outlet ($x = L$) creates a transient wave whose speed is $a = 1{,}403$ m/s; the constant pressure head $H_{\text{in}} = 150$ m is maintained at the pipe's inlet ($x = 0$). The pipe is assumed to be intact, that is, $Q_{\text{leak}} = 0$. The time required for the contact discontinuity to travel from the valve back to the inlet is $\tau = L/a = 2.14$ s, and the time required for the contact discontinuity to reach the point of interest (sensor) $x^\star = L/2 = 1{,}500$ m is $\tau^\star = (L - x^\star)/a = 1.07$ s. The simulation time horizon is set to $T = 5$ s, which covers the first two contact discontinuities passing through the sensor. The uncertain initial velocity u_0 is modeled as a lognormal random variable such that $u_0 = 2.0 + 0.1 \exp z$, where z is a Gaussian random variable with mean $\mu_z = 0$ and standard deviation $\sigma_z = 0.4$. This translates into the mean $\mu_{u_0} = 2.1$ m/s and standard deviation $\sigma_{u_0} = 0.045$ m/s of the lognormal initial velocity u_0, such that 96% of the values of u_0 fall between 2.0 and 2.2 m/s.

We use a set of 30,000 Monte Carlo realizations as a yardstick against which the accuracy and computational efficiency of the method of distributions are ascertained. For each realization of u_0, the interval $(0, L)$ is discretized into 60 elements and the WHE (1) are solved using the method of characteristics with the explicit finite-difference method (Chaudhry, 2013; Wylie et al., 1993). Monte Carlo estimates of the PDFs of $h(x,t)$ and $u(x,t)$ are obtained using a Gaussian kernel density estimator provided by the Matlab function ksdensity, which automatically estimates the kernel density estimator bandwidth. The sampling errors in computing the mean ($\mathcal{E}_{\bar{h}}$) and variance ($\mathcal{E}_{\sigma_h^2}$) of $h(x^\star, t = 3.14\text{s})$ from N_{MC} Monte Carlo realizations ($N_{\text{MC}} \leq 30{,}000$), as well as the corresponding errors $\mathcal{E}_{\alpha_1}$ and $\mathcal{E}_{\alpha_2}$ in estimating the mixed ensemble moments α_1 and α_2, are defined as

$$\mathcal{E}_{\mathcal{A}}(N_{\text{MC}}) = \left| \frac{\mathcal{A}(30000) - \mathcal{A}(N_{\text{MC}})}{\mathcal{A}(30000)} \right|, \qquad \mathcal{A} = \bar{h}, \sigma_h^2, \alpha_1, \alpha_2. \tag{6}$$

A sampling error in estimation of $f_h(H; x^\star, t = 3.14\text{s})$, the PDF of $h(x^\star, t = 3.14\text{s})$, is reported in terms of the Kullback-Leibler (KL) divergence between $f_h(H; x^\star, t = 3.14\text{s})$ estimated from 30,000 Monte Carlo realizations of $h(x^\star, t = 3.14\text{s})$, $f_{h,30000}$, which is treated as ground truth, and its counterpart computed with a smaller number of realization N_{MC}, $f_{h,N_{\text{MC}}}$. The latter is defined as

$$\mathcal{E}_{f_h}(N_{\text{MC}}) \equiv D_{\text{KL}}(f_{h,N_{\text{MC}}}, f_{h,30000}) \equiv \int f_{h,N_{\text{MC}}} \ln\left(\frac{f_{h,N_{\text{MC}}}}{f_{h,30000}}\right) \mathrm{d}H. \tag{7}$$

As expected, all five sampling errors in (6) and (7) decrease as the number of Monte Carlo realizations N_{MC} increases (Figure 2). The sampling errors in estimating the means, $\bar{h}$ and $\bar{u}$, and the closure variable α_1 fall below 10^{-3} after $N_{\text{MC}} \approx 1{,}000$ realizations, while no fewer than $N_{\text{MC}} = 30{,}000$ realizations are required to estimate the PDFs of h and u with the same accuracy. While the sampling error $\mathcal{E}_{\alpha_2}(N_{\text{MC}} = 1{,}000) = \mathcal{O}(10^{-2})$, its effect on the overall predictive error is diminished by the fact that α_2 in (3)–(5) is multiplied by $(U - \bar{u})$ which, during the time period of significance for leak detection tests (see below), is $\mathcal{O}(10^{-2})$. Since only $\bar{u}, \bar{h}, \alpha_1$, and α_2 are used in the PDF equations (3)–(5), the use of the latter to obtain PDFs results in significant computation saving.

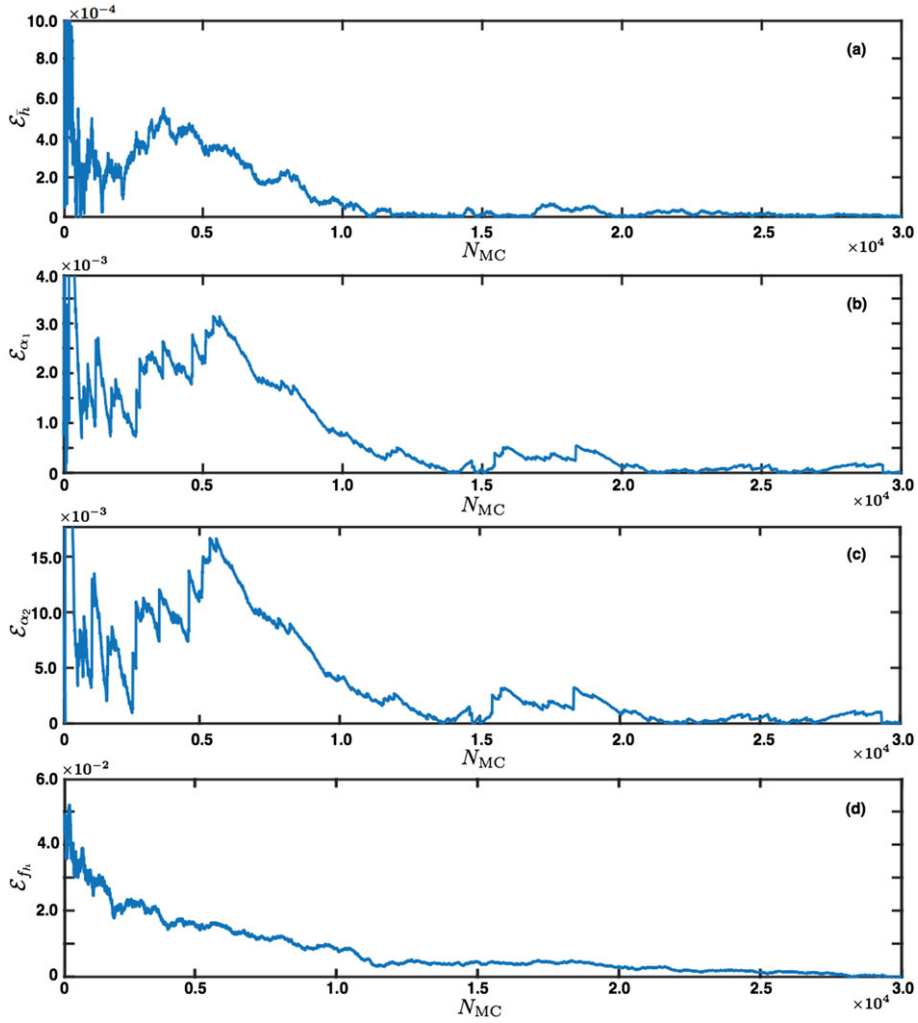

Figure 2. Sampling errors in estimating, from N_{MC} Monte Carlo realizations, the sample mean (a) and probability density function (d) of the pressure head h in the middle of the pipe ($x = 1{,}500$ m) after the first contact discontinuity passed through it (at time $t = 3.14$ s). Also shown are the corresponding sampling errors in estimating the closure variables α_1 (b) and α_2 (c). All the errors are defined in (6) and (7).

The coefficients in the PDF equations (3)–(5) exhibit jump discontinuities at space-time points wherein the forward and backward waves traveling along the corresponding two families of characteristics intersect (see Appendix C for detail). These discontinuities can be handled either with an appropriate numerical method or, as we do in Appendix C for the leak-free flows, analytically by taking advantage of the fact that their dynamics are deterministic.

Figure 3 exhibits the marginal PDF $f_h(H, x^\star, t)$ for the pressure head $h(x, t)$ in the sensor location, $x^\star = L/2$, before the first contact discontinuity (a), after the first contact discontinuity (b), and after the second contact discontinuity (c) pass through it. These PDFs are alternatively computed with the PDF method and MCS comprising $N_{MC} = 1{,}000$ and $N_{MC} = 30{,}000$ realizations. The solution of the PDF equation, whose parametrization relies on $N_{MC} = 1{,}000$ realizations, agrees with the PDF estimate based on $N_{MC} = 30{,}000$ realizations: The difference between these two solutions, as quantified by the KL divergence, is $\mathcal{E}_{f_h} = 0.0017$. The MCS estimate of f_h achieves the same accuracy with $N_{MC} \approx 6{,}000$ realizations, which takes about three times longer to compute than the PDF method does. If one were to rely on the Kolmogorov-Smirnov test, $\mathcal{E}^{KS}_{f_h} = \sup_H |f_{h,N_{MC}} - f_{h,30000}|$, as a measure of the difference between the "exact" and approximate PDFs then the PDF method is nine times faster than MCS (one needs $N_{MC} \approx 19{,}000$ realizations to achieve the error $\mathcal{E}^{KS}_{f_h} = 0.0016$ of the PDF method), with an even larger computational gain. The comparison between the PDF estimates provided by the PDF

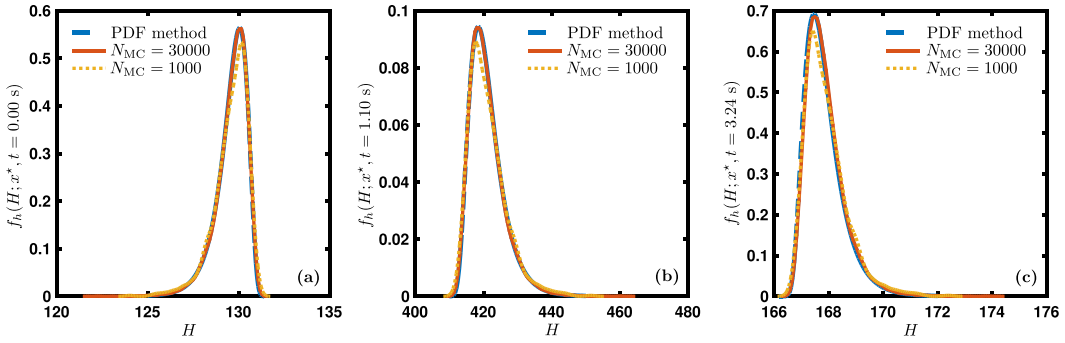

Figure 3. Temporal snapshots of the PDF $f_h(H; x^\star, t)$ of the pressure head $h(x, t)$ at the observation point $x = x^\star$ obtained analytically in Appendix C (dashed line) or by using the kernel density estimator to postprocess $N_{MC} = 30{,}000$ (solid line) and $N_{MC} = 1{,}000$ (dotted line) Monte Carlo realizations. The results are presented at $x^\star = L/2$ (the middle of the pipe), for three times t: at initial time $t = 0.00$ s (a); and the times $t = 1.10$ s (b) and $t = 3.24$ s (c) at which the first and second contact discontinuities pass over $x^\star$, respectively. PDF = probability density function.

method and MCS with $N_{MC} = 30{,}000$ realizations in Figures 3 and 4 validates the accuracy of the closure approximation, which underpins the derivation of our deterministic PDF equation (4).

The support of the PDF $f_h(H; \cdot)$, that is, a set of values of H for which $f_h(H; \cdot) \neq 0$, changes with time; the predictive uncertainty (pressure variance σ_h^2 or the PDF width) is significantly larger after the passage of the first contact discontinuity (Figure 3b) than the second one (Figure 3c). That is why many leak-detection techniques focus on the time interval after the first contact discontinuity to determine the leak location and size, taking advantage of the fact that during this time the pressure is highest and the effects of a leak are magnified (Covas et al., 2008). Damping in the periodic wave gives the first cycle the advantage over the other cycles since the leak effect is at its peak. In general, the pressure PDF f_h and its moments (e.g., the mean and variance of h) are discontinuous at the moving wave front. In between the two adjacent waves carrying, for example, the first and second contact discontinuities, the pressure $h(x, t)$ is continuous and the impact of uncertain parameters increases with time (Figure 4); therefore, pressure (and velocity) measurements collected during that time interval have higher information content (i.e., their assimilation would have a higher impact on reduction of the predictive uncertainty) than the data collected at other times.

The fluid pressure PDF $f_h(H; \cdot)$ remains highly asymmetric (non-Gaussian) at all times, with skewness that changes sign during the time cycle considered (Figure 3). This suggests that data assimilation strategies based on different flavors of the Kalman filter are suboptimal and might yield erroneous estimators of the system states and inputs (e.g., the location and intensity of a leak). Instead, one might have to deploy Bayesian strategies, which would treat the PDF $f_h(H; \cdot)$ computed with our PDF equations as a prior distribution and then use pressure measurements to construct a posterior PDF.

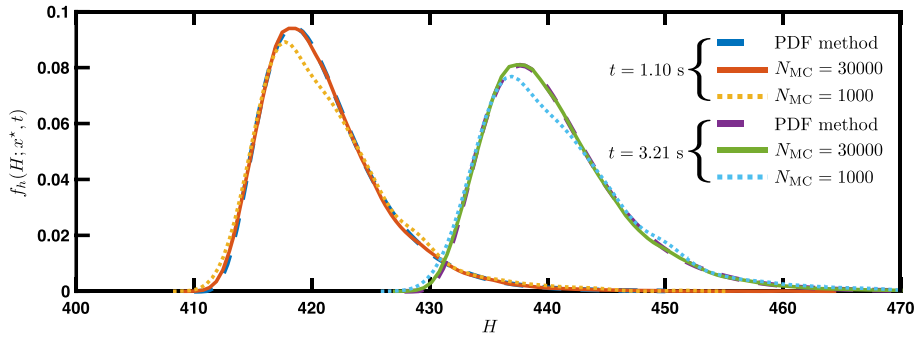

Figure 4. Temporal snapshots of the PDF $f_h(H; x^\star, t)$ of the pressure head $h(x, t)$ at the observation point $x = x^\star$ obtained, alternatively, by solving the PDF equation (4) (dashed line) or by using the kernel density estimator to postprocess $N_{MC} = 30{,}000$ (solid line) and $N_{MC} = 1{,}000$ (dotted line) Monte Carlo realizations. The results are presented at $x^\star = L/2$ (the middle of the pipe) for the time interval during which the first contact discontinuity passed through $x^\star$ ($t = 1.10$ s) and just before the second contact discontinuity has reached it ($t = 3.21$ s). PDF = probability density function.

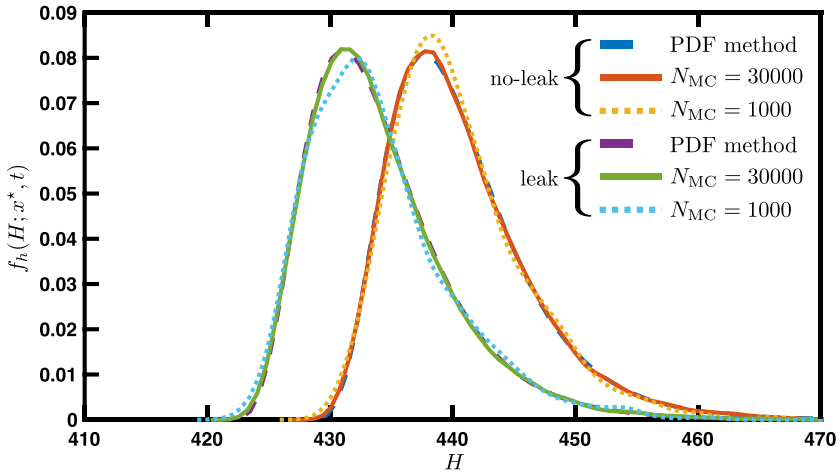

Figure 5. Temporal snapshots of the PDF $f_h(H;x,t)$ of the pressure head $h(x,t)$ for an intact pipe and a pipe with leak at point x_{leak} = 2,450 m with uncertain initial conditions. The results are presented at the middle of the pipe, $x = x^\star$, at time t = 3.21 s. PDF = probability density function.

The PDFs in Figures 3 and 4 quantify the uncertainty in predictions of the fluid pressure dynamics stemming from uncertain initial conditions in an intact pipe. In the presence of a leak, the pressure signals typically display faster damping and more complex wave reflections. Figure 5 demonstrates this effect by comparing the pressure PDFs in leaky and intact pipes; in both cases the initial velocity is set to u_0 = 2.1 m/s and, for the leaky pipe, the leak parameter is set to $C_{leak}A_{leak} = 0.0001$ m^2. The PDF behavior is significantly affected by the presence of the leak, the most apparent feature being a significant shift of the PDF towards lower-pressure values.

Comparison of the PDFs in leak and no-leak conditions might help one to identify locations where the leak effects are most pronounced. These locations are also most advantageous for data collection, i.e., sensor placement, since the discrepancy between observations and the predicted PDFs would be largest in the presence of a leak. In all other cases, it represents a physically based prior distribution to be updated via data assimilation for uncertainty reduction and possibly leak detection.

5. Conclusions

We developed a deterministic partial-differential equation for the joint PDF of the fluid pressure and flow velocity in a pipe. The latter are governed by the WHE for hydraulic transients following the valve shut-down. Our probabilistic approach accounts for uncertainty in initial and boundary conditions for the system, and represents a computationally efficient alternative to MCS.

The closure of the PDF equation relies on the knowledge of the time evolution of the first and second moments (i.e., the mean and variance of pressure and velocity) in a specific location along the pipe. We demonstrated how using a subset of MCSs to compute the moments (and consequently the closures) for the PDF equation yields the same accuracy in the PDF estimated as obtained via MCS using the full set of realizations, resulting in significant computational savings.

The (joint) PDF obtained as a solution of the PDF equation represents a physically based prior distribution for pressure and/or velocity, which lends itself to assimilation of flowmeters and pressure transducers measurements. Data can thus be used for parameter identification and for leakage/blockage detection.

Appendix A: Derivation of PDF Equations

The derivation of a PDF equation starts by defining a "raw" PDF function (Tartakovsky & Gremaud, 2015),

$$\Pi(U-u, H-h) = \delta[U-u(x,t)]\delta[H-h(x,t)], \tag{A1}$$

where $\delta(\cdot)$ is the Dirac delta function. Its ensemble mean, over the realization of random variables u and h at

the space-time point (x, t), is the joint PDF $f_{uh}(U, H; x, t)$:

$$\mathbb{E}[\Pi] \equiv \int_{-\infty}^{\infty}\int_{-\infty}^{\infty} \delta(U-\mathcal{U})\delta(H-\mathcal{H}) f_{uh}(\mathcal{U},\mathcal{H};x,t)\mathrm{d}\mathcal{H}\mathrm{d}\mathcal{U} = f_{uh}(U,H;x,t). \tag{A2}$$

Recalling the sifting property of the Dirac delta function, $r(u)\delta(U-u) = r(U)\delta(U-u)$; noting that

$$\frac{\partial \Pi}{\partial t} = \frac{\partial \Pi}{\partial h}\frac{\partial h}{\partial t} + \frac{\partial \Pi}{\partial u}\frac{\partial u}{\partial t} = -\frac{\partial \Pi}{\partial H}\frac{\partial h}{\partial t} - \frac{\partial \Pi}{\partial U}\frac{\partial u}{\partial t}; \tag{A3}$$

multiplying (1a) by $-\partial\Pi/\partial H$ and (1) by $-\partial\Pi/\partial U$; and adding the resulting equations together lead to

$$\frac{\partial \Pi}{\partial t} - \frac{\partial \Pi}{\partial H}\frac{a^2}{g}\frac{\partial u}{\partial x} - \frac{\partial \Pi}{\partial U} g\frac{\partial h}{\partial x} = -\frac{\partial}{\partial U}[r(U)\Pi] - \delta(x-x_{\text{leak}})\frac{\partial Q_{\text{leak}}(H)\Pi}{\partial H}. \tag{A4}$$

Because of Reynolds' decompositions of the variables involved, including $\Pi = f_{uh} + \Pi'$, the ensemble mean of this equation is

$$\frac{\partial f_{uh}}{\partial t} + \frac{\partial}{\partial H}\left[Q_1 - \frac{a^2}{g}\frac{\partial \bar{u}}{\partial x} f_{uh} + Q_{\text{leak}}(H)\delta(x-x_{\text{leak}}) f_{uh}\right] + \frac{\partial}{\partial U}\left[Q_2 - g\frac{\partial \bar{h}}{\partial x} f_{uh} + k|U|U f_{uh}\right] = 0 \tag{A5}$$

where

$$Q_1 = -\frac{a^2}{g}\mathbb{E}\left[\frac{\partial u'}{\partial x}\Pi'\right] \qquad \text{and} \qquad Q_2 = -g\mathbb{E}\left[\frac{\partial h'}{\partial x}\Pi'\right]. \tag{A6}$$

As a closure approximation, we postulate that

$$Q_1 = \alpha_1(x,t)[H-\bar{h}(x,t)]f_{uh} \qquad \text{and} \qquad Q_2 = \alpha_2(x,t)[U-\bar{u}(x,t)]f_{uh}. \tag{A7}$$

The coefficients $\alpha_1(x,t)$ and $\alpha_2(x,t)$ are obtained by ensuring that the PDF f_{uh} in (A5) has the same means, $\bar{u}$ and $\bar{h}$, and variances, σ_u^2 and σ_h^2, as those resulted from the moment differential equations (B3), (B4), (B7), and (B8). To derive an expression for $\alpha_1(x,t)$, we recall that $f_h(H;x,t) = \int f_{uh}\mathrm{d}U$ so that the integration of (A5) with (A7) over U yields an equation for $f_h(H;x,t)$,

$$\frac{\partial f_h}{\partial t} + \frac{\partial}{\partial H}\left[\alpha_1(H-\bar{h})f_h - \frac{a^2}{g}\frac{\partial \bar{u}}{\partial x} f_h + Q_{\text{leak}}(H)\delta(x-x_{\text{leak}})f_h\right] = 0, \tag{A8}$$

which relies on the boundary condition $f_{uh}(\pm\infty, H; x, t) = 0$. We rely on a truncated Taylor expansion around the mean value to approximate

$$\mathbb{E}[\sqrt{h}] \approx \sqrt{\bar{h}} - \frac{\sigma_h^2}{8\bar{h}\sqrt{\bar{h}}} \qquad \text{and} \qquad \mathbb{E}[\sqrt{h}h] \approx \bar{h}\sqrt{\bar{h}} + \frac{3\sigma_h^2}{8\sqrt{\bar{h}}}.$$

Moreover, since $\int_{-\infty}^{\infty} f_h \mathrm{d}H = 1$ and $\int_{-\infty}^{\infty} H f_h \mathrm{d}H = \bar{h}$, and since $f_h(\pm\infty; x, t) = 0$ such that $\lim_{H\to\pm\infty}[H f_h(H;x,t)] = 0$, multiplying the above equation by H and integrating it over H lead to (B3). This means that the closure for Q_1 preserves the mean, regardless of the choice of $\alpha_1(x,t)$. To compute the variance of f_h, that is, $\sigma_h^2 = \int_{-\infty}^{\infty}(H-\bar{h})^2 f_h \mathrm{d}H$, we multiply (A8) by $(H-\bar{h})^2$ and integrate over H. This gives an equation for the variance,

$$\frac{\partial \sigma_h^2}{\partial t} - 2\alpha_1\sigma_h^2 = \frac{\gamma_{\text{leak}}\sigma_h^2}{\sqrt{\bar{h}}}\delta(x-x_{\text{leak}}). \tag{A9}$$

For this equation to be consistent with (B7), the coefficient α_1 in the closure approximation (A7) has to be

$$\alpha_1 = -\frac{1}{2\sigma_h^2}\beta_1. \tag{A10}$$

Combining this with the expression for β_1 derived in Appendix B leads to (3c).

Determination of $\alpha_2(x,t)$ follows a similar procedure. An equation for the marginal PDF $f_u(U;x,t) = \int f_{uh}\mathrm{d}H$ is derived by integrating (A5) with (A7) over H, while accounting for the boundary conditions $f_{uh}(U, \pm\infty; x, t) = 0$,

$$\frac{\partial f_u}{\partial t} + \frac{\partial}{\partial U}\left[\alpha_2(x,t)(U-\bar{u})f_u - g\frac{\partial \bar{h}}{\partial x} f_u + k|U|U f_u\right] = 0. \tag{A11}$$

Multiplying this equation with U, integrating the result over U, and accounting for the boundary condition, $f_u(\pm\infty; x, t) = 0$, yield

$$\frac{\partial \bar{u}}{\partial t} + g\frac{\partial \bar{h}}{\partial x} - \int_{-\infty}^{\infty} k|U|Uf_u \mathrm{d}U = 0. \tag{A12}$$

Expanding $\mathbb{E}[|u|u]$ into the truncated Taylor series (B1), we obtain $\mathbb{E}[|u|u] \approx |\bar{u}|\bar{u} + \mathrm{sgn}(\bar{u})\sigma_u^2$, so that (A12) reduces to (B4) for any choice of $\alpha_2(x, t)$. Multiplying (A11) by $(U - \bar{u})^2$ and integrating over U result in

$$\frac{\partial \sigma_u^2}{\partial t} - 2\alpha_2\sigma_u^2 = 2k\mathbb{E}[|u|u^2] - 2k\bar{u}\mathbb{E}[|u|u]. \tag{A13}$$

The second-order Taylor expansions $\mathbb{E}[|u|u] \approx |\bar{u}|\bar{u} + (|\bar{u}|/\bar{u})\sigma_u^2$ and $\mathbb{E}[|u|u^2] \approx |\bar{u}|\bar{u}^2 + 3k|\bar{u}|\sigma_u^2$ reduce (A13) to

$$\frac{\partial \sigma_u^2}{\partial t} - 2\alpha_2\sigma_u^2 = 4k|\bar{u}|\sigma_u^2. \tag{A14}$$

This variance equation is consistent with (B8) if

$$\alpha_2 = -\frac{1}{2\sigma_u^2}\beta_2. \tag{A15}$$

Combining this with the expression for β_2 derived in Appendix B leads to (3).

Appendix B: Derivation of Moments Equations

We use the Reynolds decomposition to represent random quantities (e.g., u) as the sums of their ensemble means (e.g., $\bar{u}$) and zero-mean random fluctuations (e.g., u'). Next we decompose the nonlinear terms $Q_{\mathrm{leak}} = \gamma_{\mathrm{leak}}\sqrt{h}$ and $r(u) = k|u|u$ in (1b) into a Taylor series about $\bar{h}$ and $\bar{u}$, respectively, such that

$$\begin{aligned} Q_{\mathrm{leak}}(h) &= Q_{\mathrm{leak}}(\bar{h}) + \frac{\mathrm{d}Q_{\mathrm{leak}}}{\mathrm{d}h}(\bar{h})h' + \frac{1}{2}\frac{\mathrm{d}^2Q_{\mathrm{leak}}}{\mathrm{d}h^2}(\bar{h})(h')^2 + \mathcal{O}(h'^3) \\ &= \gamma_{\mathrm{leak}}\sqrt{\bar{h}} + \frac{\gamma_{\mathrm{leak}}}{2\sqrt{\bar{h}}}h' - \frac{\gamma_{\mathrm{leak}}}{8\bar{h}\sqrt{\bar{h}}}(h')^2 + \mathcal{O}(h'^3) \end{aligned} \tag{B1}$$

$$r(u) = r(\bar{u}) + \frac{\mathrm{d}r}{\mathrm{d}u}(\bar{u})u' + \frac{1}{2}\frac{\mathrm{d}^2r}{\mathrm{d}u^2}(\bar{u})(u')^2 + \mathcal{O}(u'^3) = k|\bar{u}|\bar{u} + 2k\frac{\bar{u}^2}{|\bar{u}|}u' + k\frac{\bar{u}}{|\bar{u}|}(u')^2 + \mathcal{O}(u'^3). \tag{B2}$$

Taking the ensemble mean of the resulting version of (1) yields

$$\frac{\partial \bar{h}}{\partial t} + \frac{a^2}{g}\frac{\partial \bar{u}}{\partial x} = \left(\gamma_{\mathrm{leak}}\sqrt{\bar{h}} - \frac{\sigma_h^2\gamma_{\mathrm{leak}}}{8\bar{h}\sqrt{\bar{h}}}\right)\delta(x - x_{\mathrm{leak}}) \tag{B3}$$

$$\frac{\partial \bar{u}}{\partial t} + g\frac{\partial \bar{h}}{\partial x} = k|\bar{u}|\bar{u} + k\frac{\bar{u}}{|\bar{u}|}\sigma_u^2. \tag{B4}$$

Subtracting these from the expanded version of (1) leads to an equation for perturbations,

$$\frac{\partial h'}{\partial t} + \frac{a^2}{g}\frac{\partial u'}{\partial x} = \left(\frac{\gamma_{\mathrm{leak}}h'}{2\sqrt{\bar{h}}} - \frac{\gamma_{\mathrm{leak}}(h')^2}{8\bar{h}\sqrt{\bar{h}}} + \frac{\gamma_{\mathrm{leak}}\sigma_h^2}{8\bar{h}\sqrt{\bar{h}}}\right)\delta(x - x_{\mathrm{leak}}) \tag{B5}$$

$$\frac{\partial u'}{\partial t} + g\frac{\partial h'}{\partial x} = 2k|\bar{u}|u' + k\frac{\bar{u}}{|u|}(u')^2 - k\frac{\bar{u}}{|\bar{u}|}\sigma_u^2. \tag{B6}$$

Multiplying (B5) by $h'(x, t)$ and (B6) by $u'(x, t)$, and taking the ensemble average of the resulting equations lead to

$$\frac{\partial \sigma_h^2}{\partial t} + \beta_1 = \frac{\gamma_{\mathrm{leak}}\sigma_h^2}{\sqrt{\bar{h}}}\delta(x - x_{\mathrm{leak}}), \qquad \beta_1 = \frac{2a^2}{g}\mathbb{E}\left[h'\frac{\partial u'}{\partial x}\right] \tag{B7}$$

$$\frac{\partial \sigma_u^2}{\partial t} + \beta_2 = 4k|\bar{u}|\sigma_u^2, \qquad \beta_2 = 2g\mathbb{E}\left[u'\frac{\partial h'}{\partial x}\right]. \tag{B8}$$

Appendix C: Initial Conditions for PDF Equation

The lognormal PDF $f_{u_0}(U)$ of the initial velocity $u_0 = 2.0 + 0.1 \ln z$ with Gaussian z is given by

$$f_{u_0}(U) = \left|\frac{\mathrm{d}z}{\mathrm{d}u_0}\right| f_z = \frac{1}{\sqrt{2\pi}(U-2)\sigma_z} \exp\left[-\frac{[\ln(10(U-2)) - \mu_z]^2}{2\sigma_z^2}\right], \qquad U > 2. \tag{C1}$$

This distribution is used as the initial condition for the PDF equation before the first contact discontinuity reaches the point of interest $x^\star$, that is, during the time interval $0 \le t < \tau^\star$. Given the deterministic relation between h_0 and u_0 in (2b), the conditional PDF $f_{h_0|u_0}$ is

$$f_{h_0|u_0}(H; U; x) = \delta(H - H_{\text{in}} - \frac{kx}{g}|U|U). \tag{C2}$$

The initial condition for the joint PDF equation (3a), defined on the time interval $0 \le t < \tau^\star$, is $f_{u_0 h_0}(U, H; x) = f_{h_0|u_0} f_{u_0}$.

An equation for characteristics of the WHE (1a),

$$\frac{\mathrm{d}x}{\mathrm{d}t} = \pm a, \tag{C3}$$

defines two families of characteristics, $x(t) = at + \xi_+$ and $x(t) = -at + \xi_-$, where the constants of integration $\xi_\pm = x(0)$ label individual characteristics within each family. Specifically, the characteristic that carries backward the first contact discontinuity originating at the moment of the valve closure, $x(0) = L$, is labeled with $\xi_- = L$ (Figure 1). The wave traveling along this characteristic, $x(t) = -at + L$, reaches the observation point $x^\star = L/2$ at time $t \equiv \tau^\star = L/(2a)$. A characteristic from the family of characteristics $x(t) = at + \xi_+$, which intersects the characteristic $x(t) = -at + L$ at the space-time point $(x^\star, \tau^\star)$, is labeled by $\xi_+ = 0$, that is, which has the equation $x(t) = at$ (Figure 1).

Along all characteristics defined by (C3), including those specified by equations $x(t) = at$ and $x(t) = -at + L$, the state variables $u(x(t), t)$ and $h(x(t), t)$ satisfy

$$\frac{\mathrm{d}u(x(t),t)}{\mathrm{d}t} = \frac{\partial u}{\partial t} \pm a\frac{\partial u}{\partial x} \qquad \text{and} \qquad \frac{\mathrm{d}h(x(t),t)}{\mathrm{d}t} = \frac{\partial h}{\partial t} \pm a\frac{\partial h}{\partial x}. \tag{C4}$$

Hence, the WHE (1a) transforms into

$$\frac{\mathrm{d}u}{\mathrm{d}t} \pm \frac{g}{a}\frac{\mathrm{d}h}{\mathrm{d}t} = k|u|u \pm \frac{g}{a}Q_{\text{leak}}\delta(x - x_{\text{leak}}), \tag{C5}$$

such that the equations with the plus and minus signs are defined along the characteristics $x(t) = at$ and $x(t) = -at + L$, respectively.

C1. PDFs of u and h at the First Contact Discontinuity

Integrating (C5) for the characteristic $x(t) = at$ from 0 to $\tau^\star$, while accounting for the initial conditions $u[x(0) = 0, t = 0] = u_0$ and $h[x(0) = 0, t = 0] = H_{\text{in}}$, yields

$$u_1 - u_0 + \frac{g}{a}(h_1 - H_{\text{in}}) = k\int_0^{\tau^\star} |u|\, u\, \mathrm{d}t + \frac{g}{a}\int_0^{\tau^\star} Q_{\text{leak}}\delta(at - x_{\text{leak}})\mathrm{d}t, \tag{C6}$$

where $u_1 = u(x^\star, \tau^\star)$ and $h_1 = h(x^\star, \tau^\star)$. In the absence of a leak ($Q_{\text{leak}} = 0$), the one-dimensional velocity u along the characteristic $x = at$ remains constant, $u = u_0 > 0$, for $t < \tau^\star$. Hence, (C6) reduces to

$$u_1 - u_0 + \frac{g}{a}(h_1 - H_{\text{in}}) = k\tau^\star u_0^2. \tag{C7}$$

Integrating (C5) on the characteristic $x(t) = -at + L$ from 0 to $\tau^\star$, while accounting for the initial conditions $u[x(0) = L, t = 0] = 0$ and $h[x(0) = L, t = 0] = H_{\text{in}} + (kL/g)u_0^2 + (a/g)u_0$ obtained from (2b), yields

$$u_1 + u_0 - \frac{g}{a}(h_1 - H_{\text{in}} - \frac{kL}{g}u_0^2) = k\int_0^{\tau^\star} |u|\, u\, \mathrm{d}t - \frac{g}{a}\int_0^{\tau^\star} Q_{\text{leak}}\delta(-at + L - x_{\text{leak}})\mathrm{d}t. \tag{C8}$$

For $Q_{\text{leak}} = 0$, the first integral on the right-hand side is approximately 0 since $u(L, 0) = 0$, which yields

$$u_1 + u_0 - \frac{g}{a}(h_1 - H_{\text{in}} - \frac{kL}{g}u_0^2) = 0. \tag{C9}$$

(The impact of this approximation on the accuracy of our PDF method is investigated via comparison with MCS.) Recalling that $L/a = 2\tau^\star$, it follows from (C7) and (C9) that

$$u_1 = -\frac{k\tau^\star}{2}|u_0^2 \qquad \text{or} \qquad u_0 = \sqrt{-\frac{2}{k\tau^\star}u_1}. \tag{C10}$$

Substituting this expression into (C7) gives the corresponding value of h_1,

$$h_1 = H_{\text{in}} + \frac{a}{g}\left(u_0 + \frac{3k\tau^\star}{2}u_0^2\right). \tag{C11}$$

Since the function $U_0 = U_0(U_1)$ in (C10) is monotonic, the PDF of $u_1, f_{u_1}(U)$ is obtained as $f_{u_1}(U) = |\mathrm{d}U_0/\mathrm{d}U_1(U)|f_{u_0}(U_0(U))$ resulting in

$$f_{u_1}(U) = \frac{1}{\sqrt{-2k\tau^\star U}}f_{u_0}(U_0(U)), \qquad U > 0. \tag{C12}$$

Given the deterministic relations between h_1 and u_1 in (C11) and between u_0 and u_1 in (C10), the conditional PDF $f_{h_1|u_1}(H; U)$ is the Dirac delta function,

$$f_{h_1|u_1} = \delta\left(H - H_{\text{in}} - \frac{a}{g}\sqrt{-\frac{2U}{k\tau^\star}} + \frac{3a}{g}U\right). \tag{C13}$$

Finally, the joint PDF for u_1 and h_1 is obtained as $f_{u_1h_1} = f_{h_1|u_1}f_{u_1}$.

C2. PDFs of *u* and *h* at the Second Contact Discontinuity

The second contact discontinuity originates at (and is reflected from) the inlet boundary $x(t) = 0$ at time $t = \tau$; it travels along the characteristic line $x(t) = at + \xi_+$ with $\xi_+ = -L$ and reaches the point $x^\star = L/2$ at time $t = 2\tau - \tau^\star$ (Figure 1). At the space-time point $(x^\star = L/2, t = 2\tau - \tau^\star)$, this characteristic line intersects with the characteristic line $x(t) = -at + \xi_-$ labeled by $\xi_- = 2L$.

The two PDEs in (C5), to be solved along the characteristics $x(t) = at - L$ and $x(t) = -at + 2L$, need boundary conditions at the space-time points $\{x(\tau) = 0, \tau\}$ and $\{x(\tau) = L, \tau\}$, respectively. The value of $h[x(t), t]$ at the point $\{0, \tau\}$ is $h[x(\tau) = 0, \tau] = H_{\text{in}}$, while the corresponding boundary value for $u[x(t), t]$ is obtained by integrating in time, from 0 to τ, the PDE (C5) along the characteristic $x(t) = -at + L$. This equation is subject to the auxiliary conditions

$$u[x(0) = L, 0] = 0, \qquad h[x(0) = L, 0] = H_{\text{in}} + \frac{kL}{g}u_0^2 + \frac{a}{g}u_0.$$

Since in the absence of the leak ($Q_{\text{leak}} = 0$), $u \approx 0$ for $t < \tau$ along the characteristics $x(t) = -at + L$, and accounting for these boundary conditions, the time integration of the respective PDE (C5) yields the required value of $u[x(t), t]$ at the point $\{0, \tau\}$,

$$u[x(\tau) = 0, \tau] = -u_0 - \frac{kL}{a}u_0^2. \tag{C14}$$

Likewise, the value of $u[x(t), t]$ at the point $\{x(\tau) = L, \tau\}$ is $u[x(\tau) = L, \tau] = 0$. The corresponding boundary value for $h[x(t), t]$ is obtained by integrating in time, from 0 to τ, the PDE (C5) along the characteristic $x(t) = at$. This equation is subject to the auxiliary conditions

$$u[x(0) = 0, 0] = u_0, \qquad h[x(0) = 0, 0] = H_{\text{in}}.$$

A solution of this boundary-value problem is

$$-u_0 + \frac{g}{a}(h[x(\tau) = L, \tau] - H_{\text{in}}) = k\int_0^\tau |u|u\mathrm{d}\tau'. \tag{C15}$$

According to the fundamental theorem of integral calculus, $\int_0^\tau g(\tau')\mathrm{d}\tau' = g(\xi)\tau$ with $0 < \xi < \tau$; as an approximation, we choose $g(\xi) = [g(0) + g(\tau)]/2$. Since $u(L, \tau) = 0$, this leads to the required value of $h[x(t), t]$ at the point $\{L, \tau\}$,

$$h[x(\tau) = L, \tau] = H_{\text{in}} + \frac{a}{g}\left(u_0 + \frac{k\tau}{2}u_0^2\right). \tag{C16}$$

With these boundary conditions, and in the absence of leaks, the initial-value problem (C5) along the characteristic $x = at - L$ is

$$\frac{\mathrm{d}u}{\mathrm{d}t} + \frac{g}{a}\frac{\mathrm{d}h}{\mathrm{d}t} = k|u|u, \qquad h[x(\tau) = 0, \tau] = H_{\text{in}}, \qquad u[x(\tau) = 0, \tau] = -u_0 - k\tau u_0^2.$$

Integrating this problem from τ to $2\tau - \tau^\star$ yields the values of u and h at the second contact discontinuity (Figure 1), $u_2 \equiv u(x^\star, 2\tau - \tau^\star)$ and $h_2 \equiv h(x^\star, 2\tau - \tau^\star)$,

$$u_2 + u_0 + k\tau u_0^2 + \frac{g}{a}(h_2 - H_{\text{in}}) = -k(\tau - \tau^\star)(u_0 + k\tau u_0^2)^2. \tag{C17}$$

This equation is derived by assuming that $u \approx u[x(\tau) = 0, \tau] = -u_0 - k\tau u_0^2$ for $\tau < t < 2\tau - \tau^\star$. Likewise, the initial-value problem (C5) along the characteristic $x = -at + 2L$ is

$$\frac{\mathrm{d}u}{\mathrm{d}t} - \frac{g}{a}\frac{\mathrm{d}h}{\mathrm{d}t} = k|u|u, \qquad h[x(\tau) = L, \tau] = H_{\text{in}} + \frac{a}{g}\left(u_0 + \frac{k\tau}{2}u_0^2\right), \qquad u[x(\tau) = L, \tau] = 0.$$

Integrating this problem from τ to $2\tau - \tau^\star$, while accounting for the fact that $u \approx 0$ for $\tau < t < 2\tau - \tau^\star$, yields

$$u_2 - \frac{g}{a}(h_2 - H_{\text{in}}) - \left(u_0 - \frac{k\tau}{2}u_0^2\right) = 0. \tag{C18}$$

A solution of (C17) and (C18) for u_2 is a fourth-degree polynomial in u_0,

$$u_2 = -\frac{k^3(\tau - \tau^\star)\tau^2}{2}u_0^4 - k^2(\tau - \tau^\star)\tau u_0^3 - k\tau u_0^2 - u_0. \tag{C19}$$

This polynomial has four roots. We approximate the root, u_0, on the interval of interest, $u_0 = 2.0 + 0.1 \ln z$ with $z \sim \mathcal{N}(0, 0.4^2)$, as

$$u_0 = \alpha u_2^2 + \beta u_2 + \gamma. \tag{C20}$$

The constants α, β, and γ are obtained by fitting (via minimization of the mean root square errors) the parabola in (C20) to the array of $\{u_{0_i}, u_{2_i}\}_{i=1}^N$ obtained from (C19). (The second-degree polynomial (C20) turned out to provide a better fit than the first-degree polynomial.) Figure C1 shows the agreement between the graphs of $u_0 = u_0(u_2)$ obtained, alternatively, from (C19) and (C20) on the domain of interest. The figure also demonstrates the agreement between these relations and the solution $u_2 = u_2(u_0)$ computed with multiple solves of the original WHE (1a) for different values of u_0. It serves to validate the approximations we have made to derive the analytical expressions for u_i and h_i with $i = 1, 2$.

Substituting (C20) into (C18) gives an expression for h_2

$$h_2 = H_{\text{in}} + \frac{a}{g}u_2 + \frac{a}{g}(\alpha u_2^2 + \beta u_2 + \gamma) + \frac{ka\tau^\star}{g}\left|\alpha u_2^2 + \beta u_2 + \gamma\right|(\alpha u_2^2 + \beta u_2 + \gamma). \tag{C21}$$

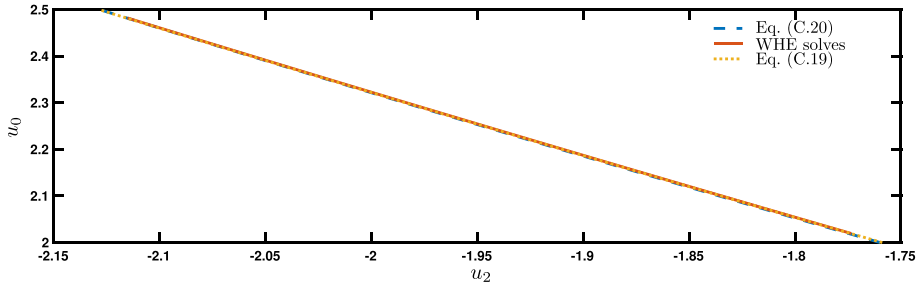

Figure C1. The relationship between u_0 and u_2 computed, alternatively, with (C19), (C20), and multiple solves of the WHE (1a) for different values of u_0. This relationship is monotonic in the region of interest. WHE = water hammer equation.

Since the function $u_0 = u_0(u_2)$ is monotonic in the region of interest (Figure C1), the corresponding PDFs are

$$f_{u_2} = \left|\frac{\mathrm{d}u_0}{\mathrm{d}u_2}\right| f_{u_0} = \frac{|2\alpha U + \beta|}{(\alpha U^2 + \beta U + \gamma - 2)\sigma\sqrt{2\pi}} \exp\left(\frac{-[\ln(10(\alpha U^2 + \beta U + \gamma - 2)) - \mu]^2}{2\sigma^2}\right) \tag{C22}$$

$$f_{h_2|u_2} = \delta\left(H - H_{\mathrm{in}} - \frac{a}{g}U - \frac{a}{g}(\alpha U^2 + \beta U + \gamma) - \frac{ka\tau^\star}{g}\left|\alpha U^2 + \beta U + \gamma\right|(\alpha U^2 + \beta U + \gamma)\right) \tag{C23}$$

$$f_{u_2 h_2} = f_{h_2|u_2} f_{u_2}. \tag{C24}$$

The same procedure can be repeated after each contact discontinuity, until $t = t_{\max}$.

Acknowledgments
This work was supported in part by the National Science Foundation under grant DMS-1802189 and by the Air Force Office of Scientific Research under grant FA9550-17-1-0417. There are no data sharing issues since all of the numerical information is provided in the figures produced by solving the equations in the paper.

References

Barajas-Solano, D. A., & Tartakovsky, D. M. (2016). Stochastic collocation methods for nonlinear parabolic equations with random coefficients. *SIAM / ASA Journal on Uncertainty Quantification*, *4*(1), 475–494.

Brothers, K. J. (2001). Water leakage and sustainable supply—Truth or consequences? *Journal - American Water Works Association*, *93*(4), 150–152.

Brunone, B., & Ferrante, M. (2001). Detecting leaks in pressurised pipes by means of transients. *Journal of Hydraulic Research*, *39*(5), 539–547.

Brunone, B., Ferrante, M., & Meniconi, S. (2008). Portable pressure wave-maker for leak detection and pipe system characterization. *Journal - American Water Works Association*, *100*(4), 108–116.

Chaudhry, M. H. (2013). *Applied Hydraulic Transients* (3rd ed.). New York: Springer.

Colombo, A. F., Lee, P., & Karney, B. W. (2009). A selective literature review of transient-based leak detection methods. *Journal of Hydro-environment Research*, *2*(4), 212–227.

Covas, D., Ramos, H., & De Almeida, A. B. (2005). Standing wave difference method for leak detection in pipeline systems. *Journal of Hydraulic Engineering*, *131*(12), 1106–1116.

Covas, D., Ramos, H., Lopes, N., & Almeida, A. B. (2008). Water pipe system diagnosis by transient pressure signals. In *Water Distribution Systems Analysis Symposium* (pp. 1–19). Cincinnati, OH.

Duan, H.-F. (2015). Uncertainty analysis of transient flow modeling and transient-based leak detection in elastic water pipeline systems. *Water Resources Management*, *29*(14), 5413–5427.

Massari, C., Yeh, T.-C. J., Ferrante, M., Brunone, B., & Meniconi, S. (2013). Diagnosis of pipe systems by the SLE: First results. *Water Science & Technology*, *13*(4), 958–965.

Massari, C., Yeh, T.-C. J., Ferrante, M., Brunone, B., & Meniconi, S. (2014). Detection and sizing of extended partial blockages in pipelines by means of a stochastic successive linear estimator. *Journal of Hydroinformatics*, *16*(2), 248–258.

Meniconi, S., Brunone, B., Ferrante, M., Capponi, C., Carrettini, C. A., Chiesa, C., et al. (2015). Anomaly pre-localization in distribution–transmission mains by pump trip: Preliminary field tests in the Milan pipe system. *Journal of Hydroinformatics*, *17*(3), 377–389.

Mpesha, W., Gassman, S. L., & Chaudhry, M. H. (2001). Leak detection in pipes by frequency response method. *Journal of Hydraulic Engineering*, *127*(2), 134–147.

Neuman, S. P., Tartakovsky, D. M., Wallstrom, T. C., & Winter, C. L. (1996). Prediction of steady state flow in nonuniform geologic media by conditional moments: Exact nonlocal formalism, effective conductivities, and weak approximation. *Water Resources Research*, *32*(5), 1479–1480. https://doi.org/10.1029/96WR00489

Sattar, A. M. A., & El-Beltagy, M. (2016). Stochastic solution to the water hammer equations using polynomial chaos expansion with random boundary and initial conditions. *Journal of Hydraulic Engineering*, *143*(2), 4016078.

Taghvaei, M., Beck, S. B. M., & Boxall, J. B. (2010). Leak detection in pipes using induced water hammer pulses and cepstrum analysis. *International Journal of COMADEM*, *13*(1), 19.

Tartakovsky, D. M., & Gremaud, P. A. (2015). Method of distributions for uncertainty quantification. In D. M. Tartakovsky & P. A. Gremaud (Eds.), *Handbook of uncertainty quantification* (pp. 763–783). New York: Springer. https://doi.org/10.1007/978-3-319-12385-1-27

Thornton, J., Sturm, R., & Kunkel, G. (2008). *Water loss control* (2nd ed.). New York: McGraw Hill.

Vítkovskỳ, J. P., Lambert, M. F., Simpson, A. R., & Liggett, J. A. (2007). Experimental observation and analysis of inverse transients for pipeline leak detection. *Journal of Water Resources Planning and Management*, *133*(6), 519–530.

Wang, X.-J., Lambert, M. F., Simpson, A. R., Liggett, J. A., & Vítkovskỳ, J. P. (2002). Leak detection in pipelines using the damping of fluid transients. *Journal of Hydraulic Engineering*, *128*(7), 697–711.

Wylie, E. B., Streeter, V. L., & Suo, L. (1993). *Fluid transients in systems* (2nd ed.)., vol. 1. NJ: Prentice Hall, Englewood Cliffs.

Ye, G., & Fenner, R. (2010). Kalman filtering of hydraulic measurements for burst detection in water distribution systems. *Journal of Pipeline Systems Engineering*, *2*(1), 14–22.

Zhang, Q., Karney, B., Suo, L., & Colombo, A. F. (2011). Stochastic analysis of water hammer and applications in reliability-based structural design for hydro turbine penstocks. *Journal of Hydraulic Engineering*, *137*(11), 1509–1521.